applied sciences

MDPI

Article

# Use of Texture Feature Maps for the Refinement of Information Derived from Digital Intraoral Radiographs of Lytic and Sclerotic Lesions

**Rafał Obuchowicz [1,*], Karolina Nurzynska [2], Barbara Obuchowicz [3], Andrzej Urbanik [1] and Adam Piórkowski [4]**

1 Department of Diagnostic Imaging, Jagiellonian University Medical College, 19 Kopernika Street, 31-501 Cracow, Poland
2 Institute of Informatics, Faculty of Automatic Control, Electronics, and Computer Science, Silesian University of Technology, Akademicka 16, 44-100 Gliwice, Poland
3 Department of Conservative Dentistry with Endodontics, Jagiellonian University Collegium Medicum, Montelupich. 4, 31-155 Cracow, Poland
4 Department of Biocybernetics and Biomedical Engineering, AGH University of Science and Technology, Mickiewicza 30, 30-059 Cracow, Poland
* Correspondence: rafalobuchowicz@su.krakow.pl; Tel.: +48-12-424-7494

Received: 17 May 2019; Accepted: 19 July 2019; Published: 24 July 2019


**Abstract:** The aim of this study was to examine whether additional digital intraoral radiography (DIR) image preprocessing based on textural description methods improves the recognition and differentiation of periapical lesions. (1) DIR image analysis protocols incorporating clustering with the k-means approach (CLU), texture features derived from co-occurrence matrices, first-order features (FOF), gray-tone difference matrices, run-length matrices (RLM), and local binary patterns, were used to transform DIR images derived from 161 input images into textural feature maps. These maps were used to determine the capacity of the DIR representation technique to yield information about the shape of a structure, its pattern, and adequate tissue contrast. The effectiveness of the textural feature maps with regard to detection of lesions was revealed by two radiologists independently with consecutive interrater agreement. (2) High sensitivity and specificity in the recognition of radiological features of lytic lesions, i.e., radiodensity, border definition, and tissue contrast, was accomplished by CLU, FOF energy, and RLM. Detection of sclerotic lesions was refined with the use of RLM. FOF texture contributed substantially to the high sensitivity of diagnosis of sclerotic lesions. (3) Specific DIR texture-based methods markedly increased the sensitivity of the DIR technique. Therefore, application of textural feature mapping constitutes a promising diagnostic tool for improving recognition of dimension and possibly internal structure of the periapical lesions.

**Keywords:** digital intraoral radiography; image preprocessing; periapical lesions; texture analysis

## 1. Introduction

The importance of assessment of periapical lesions in clinical decision-making is well known. Osteolytic lesions form as periapical lesions in response to inflammatory infiltrates and are often associated with morbidity of the root canal pulp [1–4]. Recognition of osteolytic changes provides important information about the viability of a tooth, which influences decision-making during the treatment process. The relevant anatomical structures themselves are often small, which hinders acquisition of adequate anatomical outline. Moreover, the relative complexity of the region is increased by the presence of superimposing structures that result in "anatomical noise". All of these factors contribute to the difficulty in recognition of bone resorption on radiographic images, which impedes

the accuracy of diagnosis using digital intraoral radiography (DIR) images and may result in periapical lesions going undetected or detection is inadequate [5–7].

All of the above-mentioned factors contribute to the relatively low sensitivity of lesion detection of 70% reportedly associated with DIR images, which is markedly less than that of cone-beam computed tomography (CBCT) [8]. While visualization of lesions on CBCT is superior to that on DIR, the radiation dose the patient is exposed to via CBCT is considerably higher than that associated with conventional radiography. Therefore, use of CBCT is questionable, especially as a follow-up modality. In the current work, we present how effective DIR image analyses are with the use of image post-processing in order to refine the acquired information.

Texture feature analysis was first used to evaluate the structure of osteoporotic bone [9–11], where fractal dimension and 13 Haralick features were used for osteoporosis classification on mandibular X-ray images [9]. Similar techniques were applied to analyze periapical bone loss [12–15], where the Gray-Level Co-occurrence Matrix and Fractal Brownian Motion Model were used for bone-loss area detection [15] and localization [12]. Numerous features formed the basis for segmentation [13] and bone loss degree measurement [14]. Other applications of texture analysis were used for periapical bone healing [16–18], where radiological assessment of treatment effectiveness of guided bone regeneration was measured. The most similar research to the presented is considered in [19,20], where the authors tried to detect the type of cyst using the Gray-Level Co-occurrence Matrix and its related properties. By using textural analysis to enhance bone representation derived from DIR images, trabecular structure may be depicted more informatively, and the shapes of different anatomical structures may be determined more accurately. Such techniques may also facilitate more precise determination of changes in the periapical bone region.

The aim of the present study was to examine the applicability of different texture analysis techniques to radiographic dental images for the refinement and possible differentiation of periapical lesions.

## 2. Materials and Methods

### 2.1. Ethics Approval and Consent to Participate

The study protocol was designed in accordance with the guidelines of the Declaration of Helsinki and the Good Clinical Practice Declaration Statement. Particular care was taken to ensure the safety of personal data, and all images were anonymized before processing. Written informed consent for the publication of clinical details and anonymized clinical images was obtained from the scientific committee and management department of the dental clinic. The usual requirement for informed consent from patients was waived in view of the retrospective nature of the research.

### 2.2. Experiment Overview

The experiment described in this work consisted of three main parts:

1. Data collection—the medical-dental data describing the lesions was gathered. In all the cases, it was assured that a quality of obtained dental images was adequate. The data was carefully scrutinized for technically improper images to be rejected. Only 12-bit images recorded in digital imaging and communications in medicine (DICOM) format were accepted. Personal information in images was concealed by special software.
2. Texture feature map computation—the digitized radiographs were of various quality, therefore some standardization was necessary. Sometimes, improving the contrast by image processing methods (e.g., histogram stretching or equalization - HISTEQ) was sufficient, yet in the presented problem it was not satisfactory. Therefore, for each image a set of texture feature maps were prepared. Those maps may also be characterized with low contrast, hence again (as in the preprocessing step) the standard methods for its improvement were applied in the post-processing stage.

3. Results evaluation—finally the data was revised by experienced radiologists whose statements were the basis for the assessment of results.

A detailed description of these three parts of the experiment is given below and is presented in Figure 1.

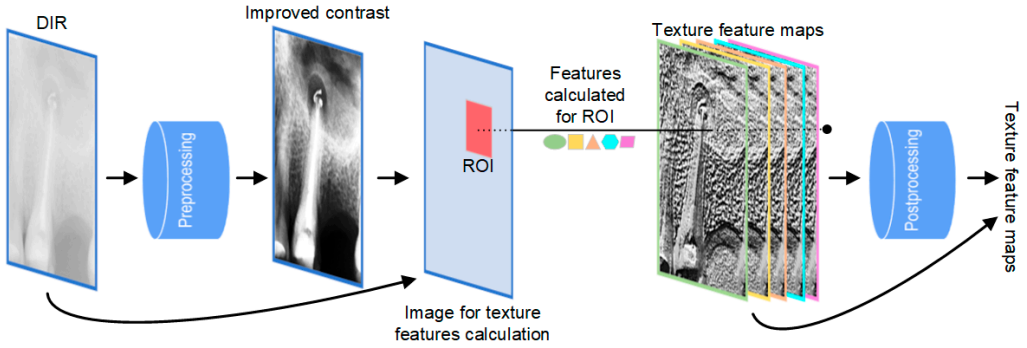


**Figure 1.** Image processing system schema. DIR, digital intraoral radiography. ROI, region of interest.

### 2.3. Dataset Description

Sixty-five anonymized DIR images from patients who attended the dental clinic from 2015 to 2017 were used in the study. Sixty-five dental DIR images, consisting of 35 images showing lytic lesions and 30 showing sclerotic lesions, were subjected to analysis. Radiographic material of patients of both sexes aged 26–57 years was used in the study. The images were selected from the institutional picture archiving and communication system (PACS). The selection criteria were acceptable image quality and suspicion of the presence of a periapical lesion on DIR.

Periapical radiographs were obtained using a dental X-ray system (Carestream Trophy with RVG 5200, Kodak, Rochester, NY, USA). Digital images were acquired at 70 kVp and 7 mA with a mean exposure time of 0.05 s, image dimensions of 1200 × 1600 pixels, and a pixel size of 0.018 mm. Digital images were saved in 16-bit digital imaging and communications in medicine (DICOM) format in the local PACS.

### 2.4. Texture Feature Map Computation

The original DIR images were analyzed using OsiriX (Pixmeo) on a Mac OS-based platform. The DIR images underwent texture preprocessing in the MATLAB environment (MathWorks, Natick, MA, USA) on Windows. The clustering of image colors was implemented using the clustering with a k-means approach (CLU). The co-occurrence matrices (COM) [21], first-order features (FOF), gray-tone difference matrices (GTDM) [22], run-length matrices (RLM) [23], and local binary patterns (LBP) [24,25] were applied. The details of the texture methods are described in [26]. Most of the mentioned methods (COM, FOF, GTDM, and RLM) in the original version compute several features to describe the whole image content. However, such an approach would not be useful for diagnostic purposes, so a new image (called a "texture feature map") reflecting the feature values calculated in a small region of interest was computed. As a consequence, several texture feature maps (depending on the number of features designed for each texture operator) were generated using this technique. In the current study, each texture feature map was generated using the "moving window" approach where, for each pixel, the new feature value was calculated on the basis of data collected in a square window (with sides of an odd number of pixels in length), to ensure that the considered pixel is in the center. In the current study, a 21 × 21 pixel square was used. This size achieves a consensus between computational overhead resulting in image processing time (which grows exponentially with the size and statistical stability of the results, where 441 elements used to fill a histogram of 256 bins is sufficient to achieve statistically reliable results) and image quality. For the LBP texture operator, the radius, R, was in a range from 3 to 15 pixels and there were 8 samples taken in the circular

neighborhood in the described experiments. In the case of clustering, from 10 up to 50 clusters were considered. The RLM calculated the matrix for images quantized to 32 and 64 colors, while the matrix stored the maximal length of 10 elements in a run. The square neighborhood applied to calculate the GTDM matrix was evaluated for sides 3, 7, and 11, yet the smallest one returned the best result. Some examples of texture feature maps achieved with the techniques described here are presented in Figure 2.

### *2.5. Pre- and Post-Processing of Images*

The DICOM images store shade information using 12 bits, the aim of which is to save as much detailed information in the scanned data as possible, while most algorithms for image processing are used to work with gray-scale images coding the information on 8 bits. Therefore, in order to process the data, the depth of the color was reduced, and the images were converted to 8-bit color coding. This operation makes it possible to compute the texture feature maps with the standard approach to texture processing and has been proven to remove some of the noise [27].

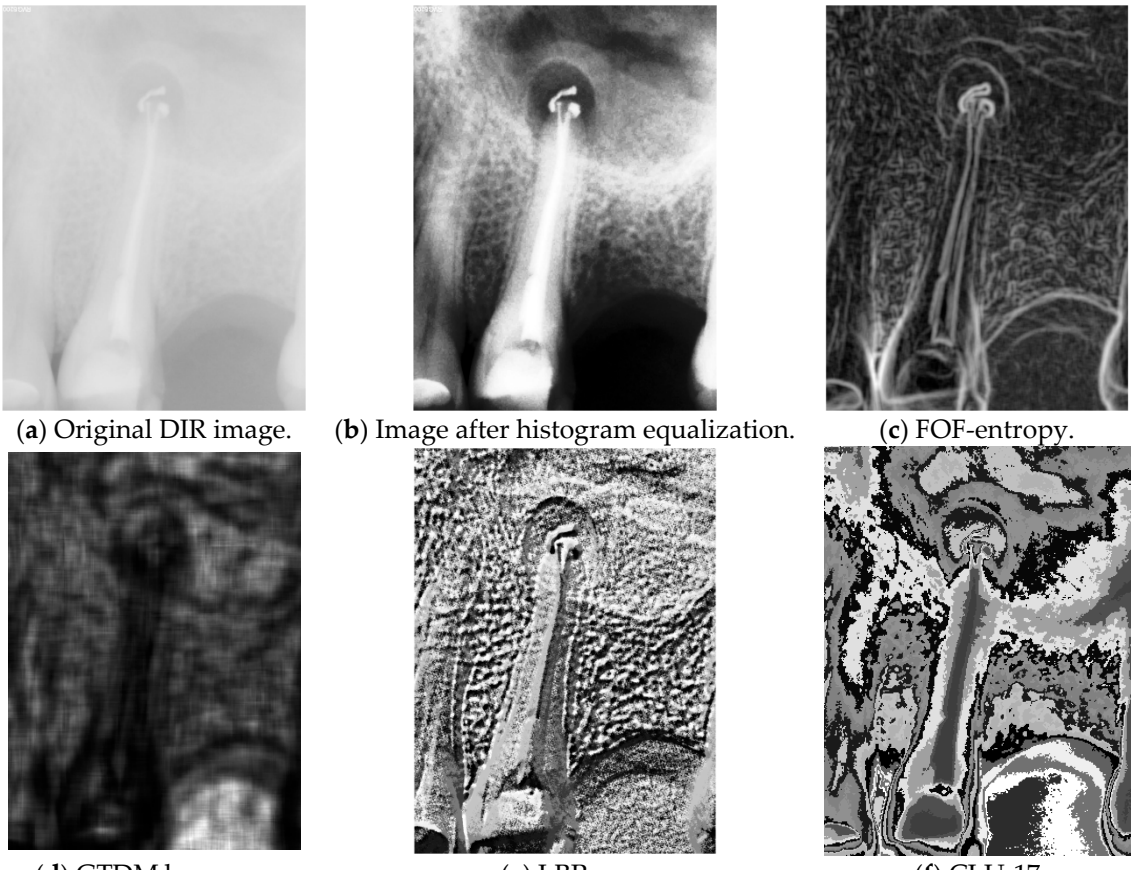

(**a**) Original DIR image. (**b**) Image after histogram equalization. (**c**) FOF-entropy.

(**d**) GTDM busyness (**e**) $LBP_{R=15}$ (**f**) CLU-17

**Figure 2.** Various aspects of image preprocessing. (**a**) Original data. (**b**) The same image after histogram equalization shows improved contrast but does not depict the structure clearly in the tooth region. (**c**–**f**) Examples of feature maps derived from a digital intraoral radiographic image via various texture analysis methods. CLU, clustering with k-means approach; DIR, digital intraoral radiography; FOF, first-order features; GTDM, gray-tone difference matrices; LBP, local binary patterns.

When an image is of low quality, particularly when it lacks sharpness and contrast, the histogram equalization operation can be applied to ensure that the whole color range is used, thereby rendering objects more easily visible, as shown in Figure 2b. However, this approach is prone to failure when used on images that contain both very dark and very light objects, as is often the case with plain radiographic

images. Hence, there is a need for more sophisticated methods to depict the data in a more informative manner. Nevertheless, application of the histogram equalization (HEQ) method in the preprocessing stage (e.g., before the texture feature map is computed) was tested, and when followed by the RLM technique, proved to be useful because the texture feature map quality improved significantly.

On the other hand, the contrast of some textural feature maps was low and did not present the content clearly. For those, histogram stretching after the final result was applied which aims in scaling the pixel values in order to assure use of the full range of 8-bit color coding (0–255). This transformation does not change the image content but makes it easier for a radiologist to evaluate. There were also some cases where application of histogram equalization gave a better effect.

### *2.6. Experiment Methodology*

The native DICOM images and texture feature maps obtained were analyzed on a 4K retina monitor by two radiologists with 10 and 30 years of experience in analysis of classical bone radiograms including dental. Standard DIR images were assessed first. The pictures were then examined separately using the techniques described above, i.e., CLU, COM, FOF, GTDM, RLM, and LBP. The prepared feature images were evaluated for radiodensity, border definition, and tissue contrast. Figure 3 presents the analyzed regions. The aforementioned parameters were estimated separately to evaluate assumptive improvement of visualization and the subsequently increased accuracy in detection of periapical lesions. Radiodensity analysis was used to evaluate bone density changes, border definition presented edge definition of the changes, and gray-scale contrast meant tissue contrast was used for evaluation of the lesion character. All features were summarized in the evaluation chart. Results were encoded in 1/0 code where 0 meant lack of the recognition of the feature and 1 meant its visual confirmation. In order to comprehensively evaluate the texture feature map usability, two main clinical issues were analyzed—sclerotic lesions and lytic lesions. Interrater reliability was at the level of 98% (on the basis of concordance correlation) where doubtful cases were established on the basis of interrater consensus.

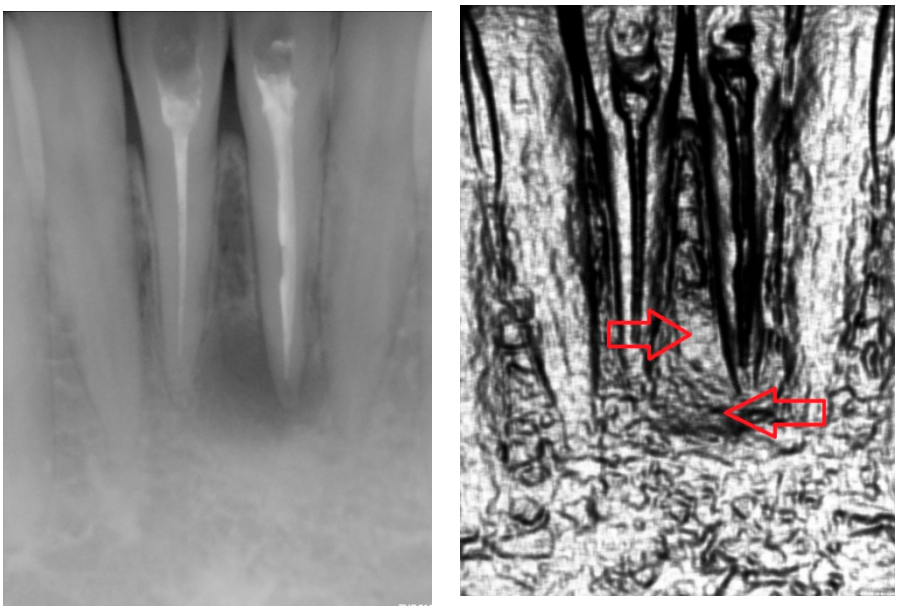

(**a**) (**b**)

**Figure 3.** *Cont.*

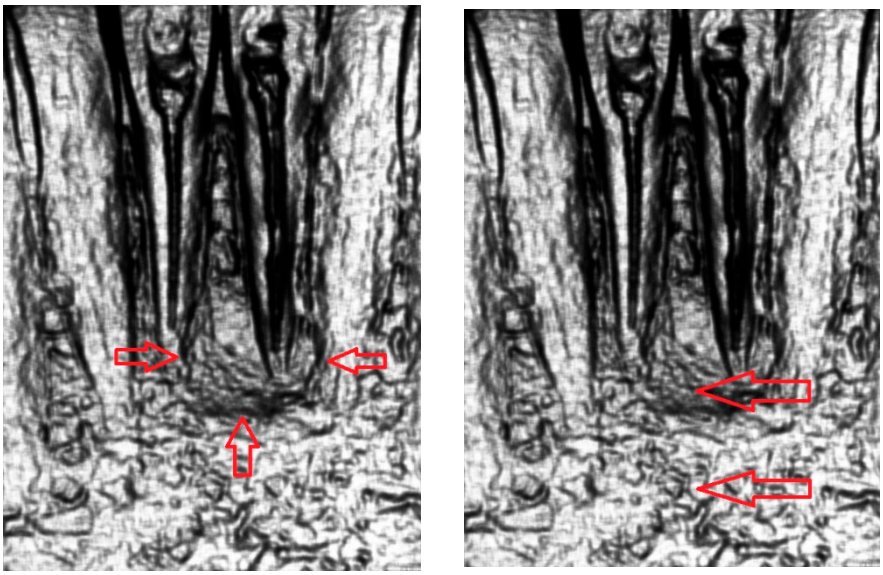

(**c**) (**d**)

**Figure 3.** Example of assessment of a periapical lesion. (**a**) Entry digital intraoral radiographic image. (**b**) Differentiation of radiodensity in the lesion (different shapes are pointed out by the arrows). (**c**) Border definition (pointed out by small arrows). (**d**) Tissue contrast between lesion and the neighborhood (shown by the arrows).

## 3. Results

Figure 4 shows the performance of each image processing approach with respect to radiological changes. The original DIR images are presented in the top row, next to the same images after histogram equalization transformation. As shown, despite the images gaining better contrast, the visibility of changes did not improve substantially. In the next row in Figure 4, the region where changes existed is enclosed within a red line. In the following rows, the texture feature maps computed for CLU, FOF energy, GTDM busyness, (HEQ) RLM, short run high gray level run emphasis, and LBP are given. Recognition of the borders of the lesions and their internal structure was markedly improved in comparison with the initial DIR image. In the FOF group, the contours of lytic changes were represented effectively. LBP and CLU revealed previously hidden information about the internal structure of the lesions and tissue contrast. (HEQ) RLM was found to improve visualization of lytic and sclerotic lesions markedly.

The delineation of sclerotic lesions and internal pattern recognition were achieved with CLU, RLM, and LBP texture feature maps.

The potential utility of each method was calculated based on data derived from experts, and changes are expressed as sensitivity and specificity for the different groups of texture feature maps that are gathered in the bar plots presented in Figure 5. All samples presenting lesions and marked as such by experts take place for true positive (TP) cases. When there was a change unnoticed by the expert, there was a true negative (TN) result. Then, when the expert noticed the change in the DIR data without lesions, a false positive (FP) result was recorded. False negative (FN) results corresponded to the situation in which the data presented any changes, and the expert confirmed it. Consequently, the formulas for sensitivity and specificity are as follows:

$$Sensitivity = \frac{TP}{TP + FN},$$

$$Specificity = \frac{TN}{TN + FP}.$$

A very low percentage value meant that the transformation did not improve visibility of a lesion, while a high percentage value indicated improved visibility and a marked increase in potential lesion recognition after texture map utilization in comparison to DIR. Performance of each image processing approach with respect to radiological changes is presented on separate graphs in Figure 5, illustrating the sensitivity and specificity of the proposed methods. Recognition and differentiation of the lytic lesions after use of the texture feature maps showed the highest sensitivity for the (HEQ) RLM texture feature map, with scores of 94%, 89%, and 94% for radiodensity, border definition, and tissue contrast, respectively; specificity for recognition of these parameters was 86%, 89%, and 43%. The next best performing texture feature map was CLU, with a sensitivity of 83%, 77%, and 80%, and a specificity of 74%, 97%, and 51% for radiodensity, border definition, and tissue contrast, respectively. FOF texture feature maps showed relatively low sensitivity for lytic lesions (60%, 69%, and 51%) but high specificity (94%, 91%, and 69%) for recognition of the three chosen radiological features.

For the sclerotic lesions, the (HEQ) RLM texture feature map was again found to have the best performance, with a sensitivity of 97%, 80%, and 97% for recognition of radiodensity, border definition, and tissue contrast, respectively. The specificity of the following texture feature maps was lower for recognition of radiodensity changes (47%) but better for border definition (90%) and tissue contrast differentiation (53%). FOF texture feature maps performed well in detection of sclerotic lesions, with recognition of radiodensity, border definition, and tissue contrast in 73%, 70%, and 57% of cases, respectively, with high specificity for the chosen features of 60%, 83%, and 73%. No important refinement of recognition of sclerotic lesions was observed for CLU texture feature maps, which had low sensitivity of values of 60%, 60%, and 3% for the three radiological features.

The highest sensitivity for detection of sclerotic lesions was shown for the (HEQ) RLM texture feature maps in terms of radiodensity differentiation, border definition, and tissue contrast recognition, but its specificity was not higher than that of the CLU and FOF texture feature maps. FOF texture feature maps showed good sensitivity for detection of sclerotic lesions and had better specificity than the CLU and RLM texture feature maps.

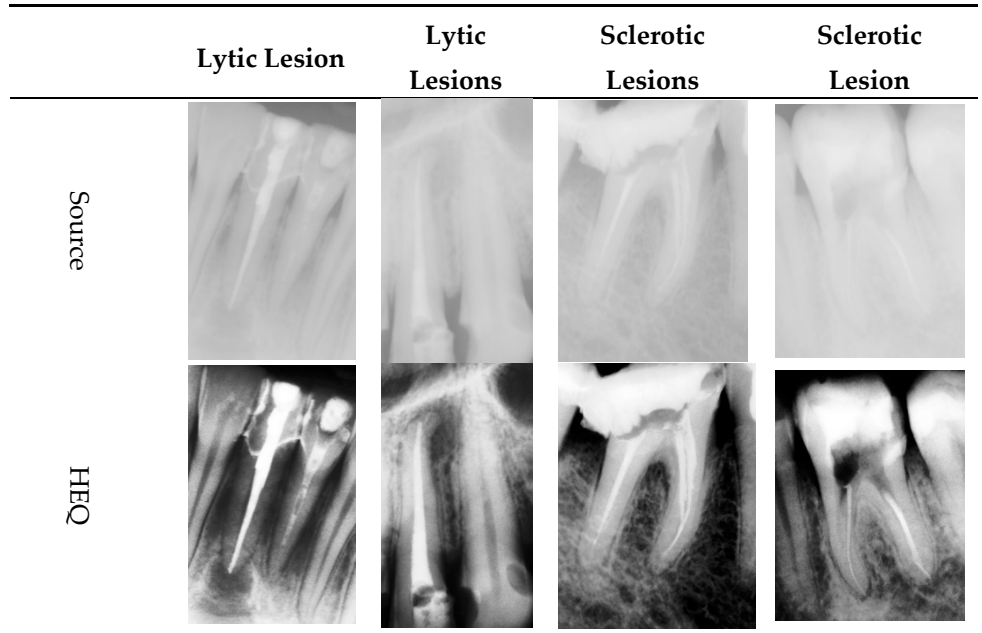


**Figure 4.** *Cont.*

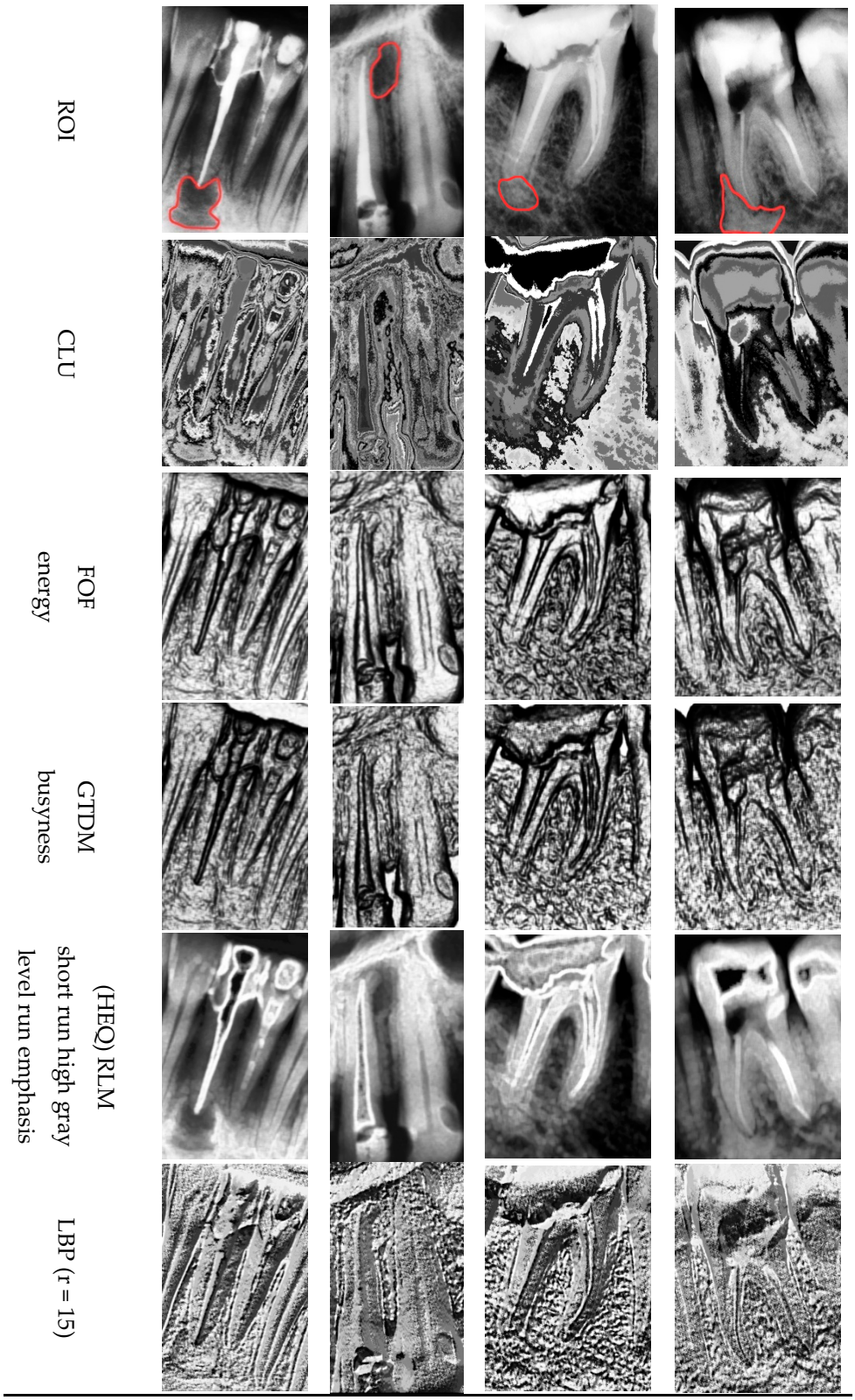


**Figure 4.** Example of assessment of a periapical lesion.

The best performance in terms of recognition of the features analyzed in both sclerotic and lytic lesions was achieved for the (HEQ) RLM texture feature map, although the FOF texture feature map showed acceptable specificity for recognition of these parameters. CLU was also a well-performing

texture feature map for detection of lytic changes, with high sensitivity but lower specificity in comparison with the FOF texture feature map (see the comparison of parameters in Figure 6).

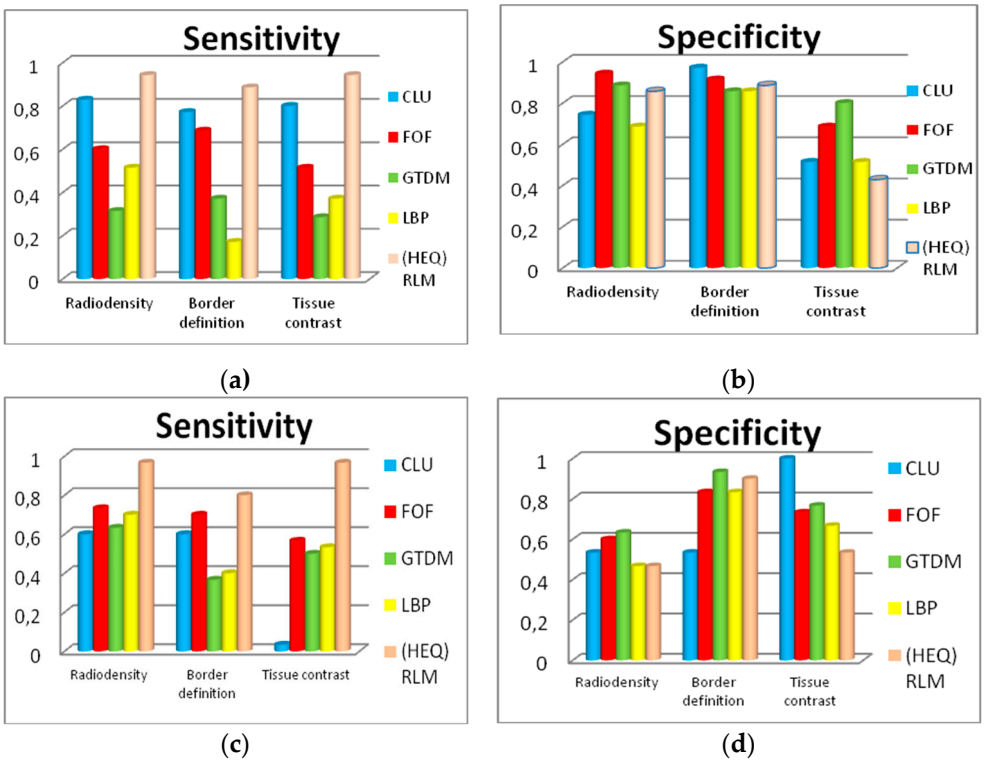


**Figure 5.** Sensitivity and specificity of different texture feature maps for detection of lytic (**a**,**b**) and sclerotic (**c**,**d**) lesions. CLU, clustering with k-means approach; FOF, first-order features; GTDM, gray-tone difference matrices; HEQ, histogram equalization; LBP, local binary patterns; RLM, run-length matrices.

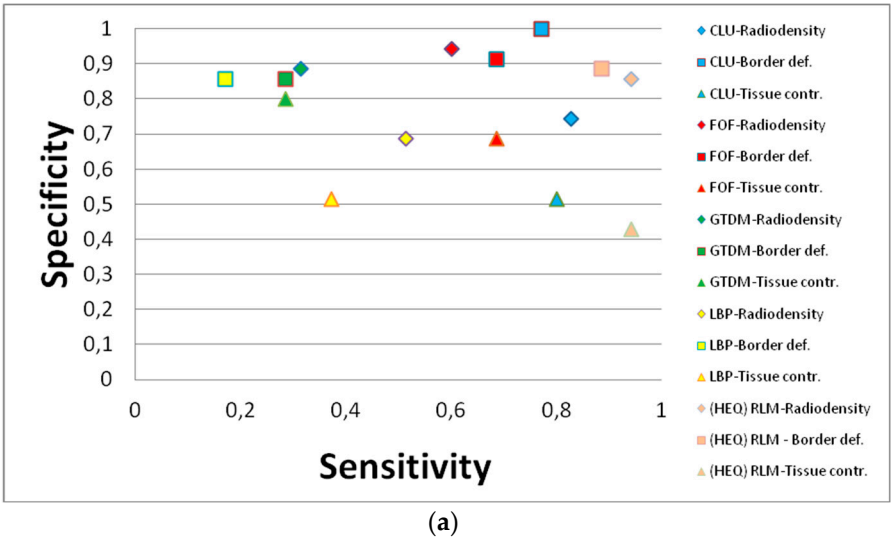


**Figure 6.** *Cont.*

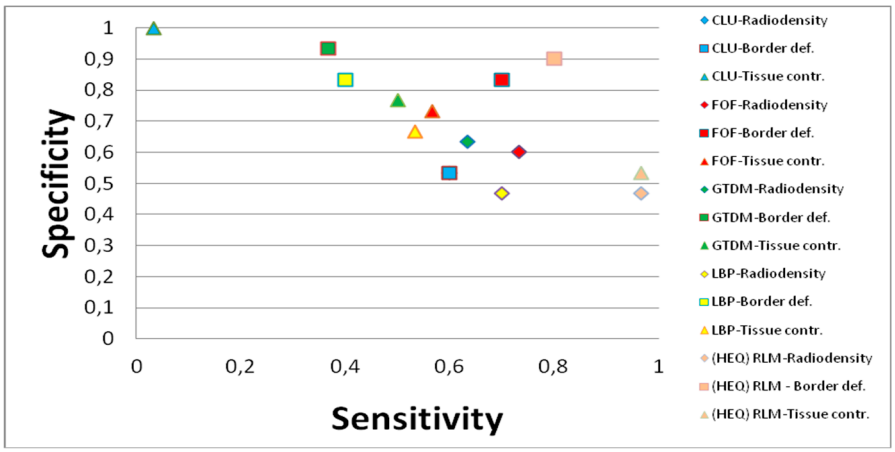


(**b**)

**Figure 6.** Relationship between specificity and sensitivity for (**a**) lytic lesions and (**b**) sclerotic lesions. Generally, the higher both values are, the better the parameter. CLU, clustering with k-means approach; FOF, first-order features; GTDM, gray-tone difference matrices; HEQ, histogram equalization; LBP, local binary patterns; RLM, run-length matrices.

## 4. Discussion

During image analysis, the observer first notices whole objects, anything that has delineated edges, and anything that is in contrast with the surrounding area. However, when the image quality is very low, the content is blurred, the image has no contrast, or an object's texture may appear very similar to that of the background. In such cases, only analysis of local differences that may be hard to discern on standard radiography may unmask some of the vital information that can be derived from the image. Although it may be impossible to detect differences by assessment of plain radiographic images, transforming visual data derived from an image with algorithms designed to map structural differences may reveal hidden content. The process used in our study is presented in Figure 2 in a sequence of images depicting how a substantial amount of additional information about a lesion was gained in comparison to the initial DIR image.

The method of using texture feature maps obtained by texture analysis of the DIR images used in the current study is consistent with that used in some previous studies [19,20]. Those methods are applicable to wide range of problems e.g., for identification of macerals [28], defect detection [29]. Moreover, there exists a MaZda system [30], which implements some of the described texture feature maps and returns similar results when compared to our implementation. Systems for differentiating cysts, ameloblastomas, and keratocysts on DIR images are described in those reports. The general approach consists of image preprocessing (e.g., opening, contrast stretching), obtaining similarity measures, and texture analysis.

In the current study, a much broader set of texture features based on different approaches to image analysis was utilized. FOF feature maps yielded significant improvements in delineation of lytic changes in comparison with DIR. GTDM enhanced visualization of the internal structure within a lytic area and important details of adjacent trabeculation with preserved lesion contours. LBP yielded a surface scene with a clearly differentiated surface pattern at the site of the lytic area. CLU increased tissue contrast in areas of lytic changes. Importantly, (HEQ) RLM increased differentiation of the border and contrast in lytic lesions but did not perform so well for sclerotic changes. Performance of different texture feature maps expressed in terms of sensitivity, specificity, F1 score, and accuracy were summarized in the Table 1 (for the lytic lesions recognition) and the Table 2 (for sclerotic lesions recognition).

**Table 1.** Sensitivity, specificity, F1 score, and accuracy in the differentiation of the different diagnostic parameters of the lytic lesions after use of texture feature maps.

| | | Sensitivity | Specificity | F1 | Accuracy |
|---|---|---|---|---|---|
| CLU | radiodensity | 0.8286 | 0.7429 | 0.7945 | 0.7857 |
| | border def | 0.7714 | 0.9714 | 0.8571 | 0.8714 |
| | tissue contr | 0.8000 | 0.5143 | 0.7000 | 0.6571 |
| FOF | radiodensity | 0.6000 | 0.9429 | 0.7241 | 0.7714 |
| | border def | 0.6857 | 0.9143 | 0.7742 | 0.8000 |
| | tissue contr | 0.5143 | 0.6857 | 0.5625 | 0.6000 |
| GTDM | radiodensity | 0.3143 | 0.8857 | 0.4400 | 0.6000 |
| | border def | 0.3714 | 0.8571 | 0.4906 | 0.6143 |
| | tissue contr | 0.2857 | 0.8000 | 0.3846 | 0.5429 |
| LBP | radiodensity | 0.5143 | 0.6857 | 0.5625 | 0.6000 |
| | border def | 0.1714 | 0.8571 | 0.2609 | 0.5143 |
| | tissue contr | 0.3714 | 0.5143 | 0.4000 | 0.4429 |
| HISTEQ-RLM | radiodensity | 0.9429 | 0.8571 | 0.9041 | 0.9000 |
| | border def | 0.8857 | 0.8857 | 0.8857 | 0.8857 |
| | tissue contr | 0.9429 | 0.4286 | 0.7500 | 0.6857 |

**Table 2.** Sensitivity, specificity, F1 score, and accuracy in the differentiation of the different diagnostic parameters of the sclerotic lesions after use of texture feature maps.

| | | Sensitivity | Specificity | F1 | Accuracy |
|---|---|---|---|---|---|
| CLU | radiodensity | 0.6000 | 0.5333 | 0.5806 | 0.5667 |
| | border def | 0.6000 | 0.5333 | 0.5806 | 0.5667 |
| | tissue contr | 0.0333 | 1.0000 | 0.0645 | 0.5167 |
| FOF | radiodensity | 0.7333 | 0.6000 | 0.6875 | 0.6667 |
| | border def | 0.7000 | 0.8333 | 0.7500 | 0.7667 |
| | tissue contr | 0.5667 | 0.7333 | 0.6182 | 0.6500 |
| GTDM | radiodensity | 0.6333 | 0.6333 | 0.6333 | 0.6333 |
| | border def | 0.3667 | 0.9333 | 0.5116 | 0.6500 |
| | tissue contr | 0.5000 | 0.7667 | 0.5769 | 0.6333 |
| LBP | radiodensity | 0.7000 | 0.4667 | 0.6269 | 0.5833 |
| | border def | 0.4000 | 0.8333 | 0.5106 | 0.6167 |
| | tissue contr | 0.5333 | 0.6667 | 0.5714 | 0.6000 |
| HISTEQ-RLM | radiodensity | 0.9667 | 0.4667 | 0.7733 | 0.7167 |
| | border def | 0.8000 | 0.9000 | 0.8421 | 0.8500 |
| | tissue contr | 0.9667 | 0.5333 | 0.7945 | 0.7500 |

Few studies of texture analysis have evaluated periapical changes. Possible differentiation of lytic lesions for granulomas and periapical cysts on the basis of radiograms with use of radiometric analysis by histogram calculation and histogram equalization were proposed by Shrout and White, respectively [31,32]. In another study, after some classic image processing methods (top hat, erosion, and opening) were performed, the skeleton was extracted, and textural features were calculated for the region of interest. A pair of pre-treatment and post-treatment values was then tested in an evaluation of the healing process [33]. The scope of such studies has typically been the detection of areas of alveolar bone on periapical dental radiographs [12–15]. These considerations were focused on segmentation, detection of lesions, and measuring the degree of alveolar bone loss rather than a textural analysis in cases requiring differentiation of lesions. A similar approach has been reported for the analysis of panoramic images in order to enhance the recognition of caries [34]. Another study assessed the treatment effectiveness of guided bone regeneration in cases of post-resectal and post-cystal bone loss on DIR images obtained using RVG 6100 digital radiography equipment (Kodak) [16]. Fractal dimension measurements (power spectral density, triangular prism surface area,

blanket, intensity difference scaling, and variogram methods) were performed, and the images became smoother during the healing process after bone loss [35].

Despite the progress to date in the quality of plain radiographic images, DIR still has a number of limitations. In addition to "anatomical noise" and small differences in bone density, there are other phenomena that impede image quality and hinder the anatomical recognition of potentially pathological structures [36,37]. Current technical developments in informatics hardware have made it possible to perform very complicated calculations in a relatively short time at low cost.

The approach used in the current study provides significantly more radiological information than standard DIR images. This comprehensive study is the first where usability of such a broad set of approaches to image texture analysis was presented. Based on our findings, from a radiological perspective, we consider these techniques a step forward in the recognition and precise localization of periapical cystic lesions. A limitation of this retrospective study is the lack of histological verification of the lesions analyzed; however, comparison of texture feature map analysis with histological results will be the issue of an upcoming study of our team. The strengths of this study include evaluation of the most popular textures known to date (mathematical transformations of image analyses applicable to DICOM-based high-resolution DIR images). Future studies should investigate the development of new image processing algorithms based on the current study, and correlations with histopathological specimens in order to evaluate their ability to predict different histologically depicted lesions on the basis of image texture.

## 5. Conclusions

The RLM texture feature map significantly improves recognition of lytic and sclerotic lesions, albeit with lower specificity for sclerotic lesions, in comparison to DIR images. CLU, in comparison to the DIR images, markedly increases visualization of lytic lesions with high sensitivity and specificity but is less able to detect the radiological features associated with sclerotic changes. FOF texture feature maps significantly improve detection of the radiological features of both sclerotic and lytic lesions, compared to DIR, with good sensitivity and specificity.

**Author Contributions:** Conceptualization, R.O., K.N. and A.P.; Data curation, R.O. and B.O.; Formal analysis, K.N.; Investigation, R.O., K.N. and A.P.; Methodology, K.N.; Project administration, A.P.; Resources, B.O.; Software, K.N.; Supervision, R.O.; Validation, R.O., B.O. and A.U.; Writing—original draft, R.O., K.N. and A.P.; Writing—review & editing, R.O., K.N., A.U. and A.P.

**Funding:** This publication was funded by AGH University of Science and Technology, Faculty of Electrical Engineering, Automatics, Computer Science and Biomedical Engineering under grant number: 16.16.120.773.

**Acknowledgments:** The authors would like to thank B. Wawrzykowska, head of the Denta-Med Kraków Clinic.

**Conflicts of Interest:** The authors declare no conflict of interest.

## References

1. Natkin, E.; Oswald, R.J.; Carnes, L.I. The relationship of lesion size to diagnosis, incidence, and treatment of periapical cysts and granulomas. *Oral Surg. Oral Med. Oral Pathol.* **1984**, *57*, 82–94. [PubMed]
2. Shrout, M.K.; Hall, J.M.; Hildebolt, C.E. Differentiation of periapical granulomas and radicular cysts by digital radiometric analysis. *Oral Surg. Oral Med. Oral Pathol.* **1993**, *76*, 356–361. [PubMed]
3. Lofthag-Hansen, S.; Huumonen, S.; Gröndahl, K.; Gröndahl, H.G. Limited cone-beam CT and intraoral radiography for the diagnosis of periapical pathology. *Oral Surg. Oral Med. Oral Pathol. Oral Radiol. Endod.* **2007**, *103*, 114–119. [PubMed]
4. Ramachandran Nair, P.N.; Pajarola, G.; Schroeder, H.E. Types and incidence of human periapical lesions obtained with extracted teeth. *Oral Surg. Oral Med. Oral Pathol. Oral Radiol. Endod.* **1996**, *81*, 93–102. [PubMed]
5. Patel, S.; Dawood, A.; Mannocci, F.; Wilson, R.; Pitt Ford, T. Detection of periapical bone defects in human jaws using cone beam computed tomography and intraoral radiography. *Int. Endod. J.* **2009**, *42*, 507–515.

6. Kolacinski, M.; Kozakiewicz, M.; Materka, A. Textural entropy as a potential feature for quantitative assessment of jaw bone healing process. *Arch. Med. Sci.* **2015**, *11*, 78–84. [PubMed]
7. Campello, A.F.; Gonçalves, L.S.; Guedes, F.R.; Marques, F.V. Cone-beam computed tomography versus digital periapical radiography in the detection of artificially created periapical lesions: A pilot study of the diagnostic accuracy of endodontists using both techniques. *Imaging Sci. Dent.* **2017**, *47*, 25–31.
8. De Paula-Silva, F.W.; Wu, M.K.; Leonardo, M.R.; Da Silva, L.A.; Wesselink, P.R. Accuracy of periapical radiography and cone-beam computed tomography scans in diagnosing apical periodontitis using histopathological findings as a gold standard. *J. Endod.* **2009**, *35*, 1009–1012.
9. Kavitha, M.S.; An, S.Y.; An, C.H.; Huh, K.H.; Yi, W.J.; Heo, M.S.; Lee, S.S.; Choi, S.C. Texture analysis of mandibular cortical bone on digital dental panoramic radiographs for the diagnosis of osteoporosis in Korean women. *Oral Surg. Oral Med. Oral Pathol. Oral Radiol.* **2015**, *119*, 346–356.
10. Harrar, K.; Jennane, R. Quantification of trabecular bone porosity on X-ray images. In Proceedings of the 4th International Conference on Industrial and Intelligent Information (ICIII 2015), Roma, Italy, 18–19 May 2015.
11. Roberts, M.G.; Graham, J.; Devlin, H. Image texture in dental panoramic radiographs as a potential biomarker of osteoporosis. *IEEE Trans. Biomed. Eng.* **2013**, *60*, 2384–2392.
12. Lin, P.L.; Huang, P.Y.; Huang, P.W.; Hsu, H.C.; Chen, P. Alveolar bone-loss area localization in periapical radiographs by texture analysis based on fBm model and GLC matrix. In Proceedings of the IEEE 2014 International Symposium on Bioelectronics and Bioinformatics, Chung Li, Taiwan, 11–14 April 2014.
13. Lin, P.L.; Huang, P.Y.; Huang, P.W.; Hsu, H.C.; Chen, C.C. Teeth segmentation of dental periapical radiographs based on local singularity analysis. *Comput. Methods Programs Biomed.* **2014**, *113*, 433–445.
14. Lin, P.L.; Huang, P.Y.; Huang, P.W. Automatic methods for alveolar bone loss degree measurement in periodontitis periapical radiographs. *Comput. Methods Programs Biomed.* **2017**, *148*, 1–11.
15. Huang, P.W.; Huang, P.Y.; Lin, P.L.; Hsu, H.C. Alveolar bone-loss area detection in periodontitis radiographs using hybrid of intensity and texture analyzed based on FBM model. In Proceedings of the International Conference on Machine Learning and Cybernetics, Lanzhou, China, 13–16 July 2014; Volume 2, pp. 487–492.
16. Borowska, M.; Szarmach, J.; Oczeretko, E. Fractal texture analysis of the healing process after bone loss. *Comput. Med. Imaging Graph.* **2015**, *46*, 191–196.
17. Borowska, M.; Bębas, E.; Szarmach, J.; Oczeretko, E. Multifractal characterization of healing process after bone loss. *Biomed. Signal. Process. Control* **2019**, *52*, 179–186.
18. Koca, H.; Ergun, S.; Guneri, P.; Boyacıoglu, H. Evaluation of trabecular bone healing by fractal analysis and digital subtraction radiography on digitized panoramic radiographs: A preliminary study. *Oral Radiol.* **2010**, *26*, 1–8.
19. Vijayakumari, B.; Ulaganathan, G.; Banumathi, A.; Banu, A.F.S.; Kayalvizhi, M. Dental cyst diagnosis using texture analysis. In Proceedings of the 2012 International Conference on Machine Vision and Image Processing, Taipei, Taiwan, 4–15 December 2012; pp. 117–120.
20. Banu, A.F.S.; Kayalvizhi, M.; Arumugam, B.; Gurunathan, U. Texture based classification of dental cysts. In Proceedings of the 2014 International Conference on Control, Instrumentation, Communication and Computational Technologies, Kanyakumari, India, 10–11 July 2014; pp. 1248–1253.
21. Haralick, R.M.; Shanmugam, K.; Dinstein, I. Textural features for image classification. *IEEE Trans. Syst. Man Cybern. Syst.* **1973**, *SMC-3*, 610–621.
22. Amadasun, M.; King, R. Textural features corresponding to textural properties. *IEEE Trans. Syst. Man Cybern. Syst.* **1998**, *19*, 1264–1274.
23. Galloway, M.M. Texture analysis using grey level run lengths. *Comput. Graph. Image Process.* **1975**, *4*, 172–179.
24. Ojala, T.; Pietikäinen, M.; Mäenpää. Grey scale and rotation invariant texture classification with local binary patterns. In *Computer Vision-ECCV 2000*; Lecture Notes in Computer Science; Springer: Berlin/Heidelberg, Germany, 2003; Volume 1842, pp. 404–420.
25. Ojala, T.; Pietikäinen, M.; Mäenpää. Multiresolution grey-scale and rotation invariant texture classification with local binary patterns. *IEEE Trans. Pattern Anal. Mach. Intell.* **2002**, *24*, 971–987.
26. Obuchowicz, R.; Nurzynska, K.; Obuchowicz, B.; Urbanik, A.; Piórkowski, A. Caries detection enhancement using texture feature maps of intraoral radiographs. *Oral Radiol.* **2019**. [CrossRef]
27. Strzelecki, M.; Kociołek, M.; Materka, A. On the influence of image features on texture classification. In *Information Technology in Biomedicine (ITIB 2018)*; Springer: Cham, Switzerland, 2018; Volume 762, pp. 15–26.

28. Skiba, M.; Mlynarczuk, M. Identification of macerals of the inertinite group using neural classifiers, based on selected textural features. *Arch. Min. Sci.* **2018**, *63*, 827–837.
29. Nurzynska, K.; Czardybon, M. Defect detection in textiles with co-occurrence matrix as a texture model description. In *International Workshop on Combinatorial Image Analysis*; Springer: Cham, Switzerland, 2018; pp. 216–226.
30. Szczypinski, P.M.; Strzelecki, M.; Materka, A.; Klepaczko, A. MaZda-A software package for image texture analysis. *Comput. Methods Programs Biomed.* **2009**, *94*, 66–76.
31. Shrout, M.K.; Hildebolt, C.E.; Vannier, M.W. Effects of region of interest (ROI) outline variations on gray-scale frequency distributions for alveolar bone. *Oral Surg. Oral Med. Oral Pathol.* **1993**, *75*, 638–644.
32. White, S.C.; Sapp, J.P.; Seto, B.G.; Mankovich, N.J. Absence of radiometric differentiation between periapical cysts and granulomas. *Oral Surg. Oral Med. Oral Pathol.* **1994**, *78*, 650–654.
33. Kim, D.; Jeong, H.; Kim, M.; Kim, C.; Lee, B.D. Multiscale image analysis for the quantitative evaluation of periapical lesion healings. In Proceedings of the 2010 3rd International Conference on Biomedical Engineering and Informatics, Yantai, China, 16–18 October 2010; Volume 1, pp. 424–427.
34. Veena, D.K.; Jatti, A.; Joshi, R.; Deepu, K.S. Characterization of dental pathologies using digital panoramic X-ray images based on texture analysis. In Proceedings of the 2017 39th Annual International Conference of the IEEE Engineering in Medicine and Biology Society (EMBC), Seogwipo, Korea, 11–15 July 2017; pp. 592–595.
35. Leite, A.F.; De Souza Figueiredo, P.T.; Caracas, H.; Sindeaux, R.; Guimaraes, A.T.B.; Lazarte, L.; De Melo, N.S. Systematic review with hierarchical clustering analysis for the fractal dimension in assessment of skeletal bone mineral density using dental radiographs. *Oral Radiol.* **2015**, *31*, 1–13.
36. Gröndahl, H.G.; Huumonen, S. Radiographic manifestations of periapical inflammatory lesions. *Endod. Topics* **2004**, *8*, 55–67.
37. Becconsall-Ryan, K.; Tong, D.; Love, R.M. Radiolucent inflammatory jaw lesions: A twenty-year analysis. *Int. Endod. J.* **2010**, *43*, 859–865.